Mechanistic study of the mechanochemical Pd^{II}-catalyzed bromination of aromatic C–H bonds by experimental and computational methods

Dajana Barišić, Ivan Halasz, Alen Bjelopetrović,
Darko Babić* and Manda Ćurić*

Division of Physical Chemistry, Ruđer Bošković Institute, Bijenička 54, HR-10000, Zagreb, Croatia

* E-mail: curic@irb.hr, dbabic@irb.hr

Abstract

An environmentally friendly approach was applied to the palladium-catalyzed halogenation of aromatic C–H bonds by *N*-halosuccinimide. Neat grinding and liquid-assisted grinding of the $Pd(OAc)_2$ precatalyst in the presence of *p*-toluenesulfonic acid in a ball mill led to the *in situ* formation of active palladium species that catalyzed the halogenation of azobenzene. Detailed insight into the mechanism of this process was obtained by *in situ* Raman monitoring, which revealed the nature of the catalytically active Pd^{II} species and intermediates and confirmed the crucial role of *p*-toluenesulfonic acid and acetonitrile as additives in the catalytic halogenation of azobenzene. By quantum-chemical (DFT) modelling of bromination of cyclopalladated azobenzene three reaction mechanisms were characterized: oxidative addition followed by reductive elimination, with neutral or protonated *N*-bromosuccinimide (NBS), and electrophilic cleavage with neutral NBS. All three mechanisms seem to be operative, with relative participation depending on the reaction conditions. Two mechanistic features were recognized in the oxidative addition of bromine to palladium atom: the biradical singlet character in the transition state realized with neutral NBS as the active species, and the barrierless migration of Br^+ with protonated NBS.

Introduction

Direct and selective replacement of inert carbon–hydrogen (C–H) bonds in arenes by carbon–halogen (C–X) bonds is of general and immense importance in organic synthesis.[1] Halogenated arenes are not only the target products but also the precursors in various organic transformations leading to further functionalization of organic compounds.[2] These transformations include the nucleophilic aromatic substitution reactions,[3] the formation of organometallic reagents,[4] and the metal-catalyzed cross-coupling reactions resulting in new carbon–carbon or carbon–heteroatom bonds.[5]

In the last two decades, ligand-directed transition-metal-catalyzed conversion of inert C–H bonds to C–X bonds or other functional groups has emerged as a superior approach[6] to traditional multi-step strategies.[7] Among the many transition metal catalysts useful for C–H bond functionalization, palladium compounds are most commonly used for such conversions.[6j] However, Pd-catalysis still relies largely on solvent-based protocols, which often require hazardous solvents, high temperatures, and long reaction times.[6]

Alternatively, the development of solid-state synthesis,[8] particularly by ball milling,[9] offers a solvent-free and environmentally friendly approach to the preparation of various classes of compounds.[10-13] In addition, ball milling reactions do not require soluble reactants, can have higher product yields and shorter reaction times than the corresponding solvent-based protocols, and may have improved reactivity and selectivity.[8-13]

The discovery of $Pd(OAc)_2$-mediated mechanochemical activation of aromatic C–H bonds in 2014[14] led to the first examples of ligand-directed transition-metal-catalyzed C–H bond functionalization under the ball milling conditions.[12b,13] Further development and application of solid-state synthesis methods for the catalytic functionalization of C–H bonds clearly requires a mechanistic understanding of these transformations.

Herein we investigate the mechanochemical Pd^{II}-catalyzed selective halogenation of azobenzene (**L**) by *N*-halosuccinimide (NXS) under environmentally benign conditions using *in situ* time-resolved Raman spectroscopy[15] and DFT calculations to understand the processes that occur during the replacement of the inert C–H bond with a C–X bond. Raman monitoring of these reactions in the presence of varied amounts of $Pd(OAc)_2$, *p*-toluenesulfonic acid (TsOH), and acetonitrile (MeCN) as solid and liquid additives, respectively, provided detailed insight into the reaction dynamics and the nature of the catalytically active palladium species and intermediates, most of which were isolated and structurally characterized.

The reaction profiles clearly showed that the halogenation of **L** proceeds via the monomeric cyclopalladated intermediate when MeCN is present or via the dimeric intermediate when MeCN is not present in the reaction mixture. Based on higher yields and faster reactions, the route via the monomeric intermediate was more efficient. Both reaction routes require the presence of TsOH, which is involved in the formation of the active Pd^{II}-catalyst and in the activation of NXS.

Three reaction mechanisms for bromination of cyclopalladated azobenzene were identified and examined by quantum-chemical (DFT) modelling. The first proceeds in two steps, oxidative addition of bromine to palladium atom and reductive elimination by 1,2-shift of bromine to the carbon atom. With electroneutral species, N-bromosuccinimide (NBS) or hydrogen bond complex NBS···*p*-TsOH, as the bromine sources, the oxidative addition must be preceded by entrance of NBS into Pd-coordination shell by replacement of another ligand (e.g. a solvent molecule). A different mechanism was determined with protonated NBS ($NBSH^+$), in which Br^+ migrates to palladium directly from free $NBSH^+$. This transfer is spontaneous, and a small barrier is present only in the subsequent elimination step. In the third mechanism, bromine migrates directly from free NBS (or from NBS···*p*-TsOH) to the activated carbon atom, with only remote assistance of the palladium atom. A distinct feature of the oxidative addition step with electroneutral species is the singlet biradical character of the transition state. All three mechanisms could be operative, with their participation depending on the reaction conditions, e.g. the presence of *p*-TsOH.

Results and discussion

To optimize the reaction conditions and to gain insight into the halogenation mechanism, we chose the bromination of **L** by *N*-bromosuccinimide (NBS) as a model reaction.

Optimization of reaction conditions.

First, we carried out the reaction of **L** and NBS in a ball mill with 5 mol% of different Pd^{II} catalysts without additives (Table 1, entries 2-5). The expected monobrominated product **LBr-I** (Scheme in Table 1) was not detected or was obtained in low yield. No reactivity was observed in the absence of the Pd^{II} catalyst (Table 1, entry 1).

Since the addition of various Brønsted acids has been demonstrated as essential for many palladium-catalyzed C–H functionalization reactions,[16,17] we tested the effect of TsOH, amidosulphonic acid (ASA), sulphanilic acid (SA) or camphorsulphonic acid (CSA) on the bromination of **L**. The presence of 0.5 equiv. of these acids led to a significant improvement in **LBr-I** yield (Table 1, entries 6-9), which increased to 59% for CSA and TsOH. Among these two acids, we chose TsOH to further optimize the reaction conditions. When the amount of TsOH was either increased to 1 equiv. or decreased to 0.25 equiv., the yield of **LBr-I** was lower (Table 1, entries 10 and 11).

Next, we explored the effect of liquid additives with different acid-base properties and proticities (acetonitrile (MeCN), H_2O, acetic acid (AcOH), *N*,*N*-dimethylformamide (DMF)), (Table 1, entries 12-16) on the bromination of **L** in the presence of TsOH and $Pd(OAc)_2$. MeCN was identified as the best liquid additive in combination with 0.5 equiv. of TsOH and 5 mol% of $Pd(OAc)_2$. Thus, after milling the reaction mixture for 2 and 3 h, the **LBr-I** was formed in 68% and 79% yields, respectively (Table 1, entries 12 and 16).

We then retested other common Pd^{II} catalysts under these optimized conditions. When $Pd(MeCN)_4(BF_4)_2$ was used instead of $Pd(OAc)_2$, almost no change in **LBr-I** yield was observed (Table 1, entry 17). On the contrary, **LBr-I** was formed in only 23% and 20% yields after replacing $Pd(OAc)_2$ with $PdCl_2$ and $PdCl_2(MeCN)_2$, respectively (Table 1, entries 18 and 19). Between $Pd(MeCN)_4(BF_4)_2$ and $Pd(OAc)_2$, we chose $Pd(OAc)_2$ to further optimize the reaction conditions because it is more stable towards air and moisture. Thus, after 4 h of milling of **L** and NBS, using 5 mol% of $Pd(OAc)_2$, with TsOH and MeCN as additives the yield increased to 83% (Table 1, entry 20). Longer milling of this mixture resulted in a slightly lower yield (Table 1, entry 21). Lower yields were also observed when the amount of $Pd(OAc)_2$ was increased to 10 mol% or decreased to 2.5 mol% (Table 1, entries 22 and 23).

Table 1 Optimization of reaction conditions[a]

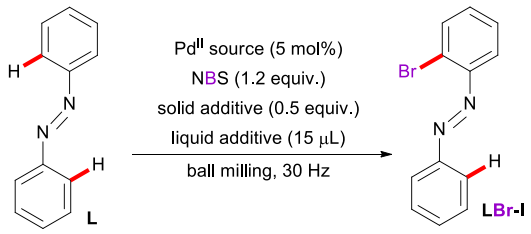

Entry	Pd^{II} source	Solid additive	Liquid additive	Time (h)	Yield[f] (%)
1	none	none	none	2	0
2	$Pd(OAc)_2$	none	none	2	4
3	$PdCl_2$	none	none	2	0
4	$PdCl_2(MeCN)_2$	none	none	2	0
5	$Pd(MeCN)_4(BF_4)_2$	none	none	2	4
6	$Pd(OAc)_2$	TsOH	none	2	59
7	$Pd(OAc)_2$	ASA	none	2	31
8	$Pd(OAc)_2$	SA	none	2	33
9	$Pd(OAc)_2$	CSA	none	2	59
10	$Pd(OAc)_2$	TsOH[b]	none	2	46
11	$Pd(OAc)_2$	TsOH[c]	none	2	49
12	$Pd(OAc)_2$	TsOH	MeCN	2	68
13	$Pd(OAc)_2$	TsOH	H_2O	2	54
14	$Pd(OAc)_2$	TsOH	AcOH	2	58
15	$Pd(OAc)_2$	TsOH	DMF	2	58
16	$Pd(OAc)_2$	TsOH	MeCN	3	79
17	$Pd(MeCN)_4(BF_4)_2$	TsOH	MeCN	3	78
18	$PdCl_2$	TsOH	MeCN	3	23
19	$PdCl_2(MeCN)_2$	TsOH	MeCN	3	20
20	**$Pd(OAc)_2$**	**TsOH**	**MeCN**	**4**	**83**
21	$Pd(OAc)_2$	TsOH	MeCN	6	78
22	$Pd(OAc)_2$[d]	TsOH	MeCN	4	74
23	$Pd(OAc)_2$[e]	TsOH	MeCN	4	56

[a]Reaction conditions: 14 mL polymethyl methacrylate (PMMA) jar, mixer mill, one nickel bound tungsten carbide milling ball (7 mm in diameter, 3.9 g), 30 Hz, **L** (0.50 mmol), Pd catalyst (5 mol%), NBS (0.60 mmol), SiO_2 (250 mg). [b]TsOH (0.5 mmol). [c]TsOH (0.125 mmol). [d]$Pd(OAc)_2$ (10 mol%). [e]$Pd(OAc)_2$ (2.5 mol%). [f]Determined by ^1H NMR spectroscopy using 1,4-dinitrobenzene as the internal standard.

Using the optimal parameters for the bromination of **L**, we further investigated the chlorination and iodination of **L** with *N*-chlorosuccinimide (NCS) and *N*-iodosuccinimide (NIS), respectively. The synthesis protocols involved milling the mixture of **L**:NXS:TsOH (1:1.2:0.5 equiv.), 5 mol% of the $Pd(OAc)_2$ precatalyst, and 15 μL of MeCN as a liquid additive. Unfortunately, the reaction of **L** with NCS gave no chlorinated product, while the reaction with NIS gave a mixture of mono- and diiodinated products at the *ortho* positions of one or both phenyl rings (**LI-I** and **LI-II**, see Section 2.2. in ESI). After milling the reaction mixture for 4 h, **LI-I** was obtained in 38% yield and **LI-II** in 43% yield. These results clearly indicate that NBS is the most effective halogen source for the selective Pd^{II}-catalyzed halogenation of the aromatic C–H bond in azobenzene.

Compared to the analogous reactions in MeCN reported by Tian and Ma,[16] the halogenation of azobenzene by ball milling significantly shortened reaction times, provided a more environmentally friendly synthetic method with an E-factor[9g] more than four times lower, and resulted in comparable yields.

Mechanistic study

Based on the optimization results and the previously established beneficial effect of TsOH and MeCN on the Pd^{II}-catalyzed functionalization reactions,[16,17] we hypothesized that $Pd(OAc)_2$ was only a precatalyst in the reactions we studied and that the catalytically active species was actually $Pd(OTs)_2(MeCN)_2$ formed *in situ*. To test this hypothesis, we prepared $Pd(OTs)_2(MeCN)_2$ by liquid-assisted grinding (LAG) and solvent-based[18] reactions from $Pd(OAc)_2$, TsOH and MeCN and tested it as a catalyst for the bromination of **L** with NBS. Indeed, $Pd(OTs)_2(MeCN)_2$ proved to be an efficient catalyst for this reaction (Table S1). The molecular structure of $Pd(OTs)_2(MeCN)_2$, resolved by PXRD analysis, reveals a *trans* configuration and the coordination by the oxygen atoms of the two tosylate ligands to the Pd^{II} center (Fig. 1 and S31).

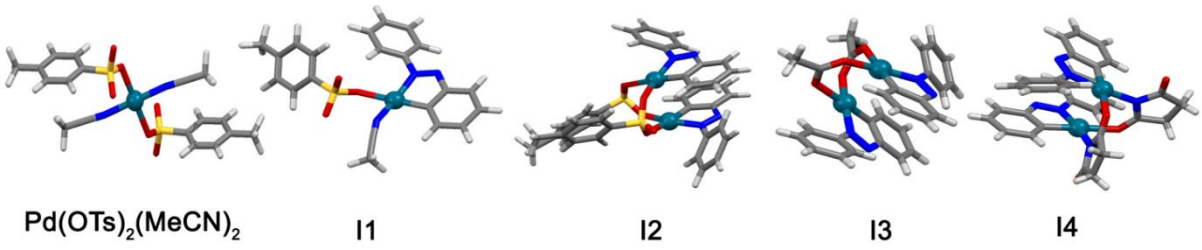

Fig. 1 Molecular structures of $Pd(OTs)_2(MeCN)_2$ catalyst and palladacycles **I1**, **I2**, **I3**,[8d] and **I4**.

To probe the possibility that bromination of **L** occurs via palladacycles resulting from C–H bond activation of **L**, we prepared tosylate palladacycles that could be intermediates in this reaction. First, we performed a series of ball-milling reactions between **L** and $Pd(OTs)_2(MeCN)_2$ or a mixture of $Pd(OAc)_2$ and TsOH with or without the addition of MeCN. Depending on the presence or absence of MeCN, the reactions led to the monomeric **I1** and dimeric **I2** palladacycles, whose structure was solved by PXRD (Fig. 1 and S32 and S33).

Apart from **I1** and **I2**, the acetate and succinimidate palladacycles **I3** and **I4** (Fig. 1) can also occur as intermediates or side products in the catalytic bromination of **L**. Therefore, the known acetate dimer[8d] **I3** was prepared by direct C–H bond activation of **L** with $Pd(OAc)_2$ in DMF vapor, while the succinimidate palladacycle **I4** was prepared by substitution of the acetates in **I3** with succinimide in a ball mill according to the recently reported method.[12d] The molecular structure of the new palladacycle **I4**, resolved by single crystal X-ray diffraction, confirmed that **I4** is a dimer with two monocyclopalladated azobenzene moieties bonded by two bridging succinimidate ligands (Fig. 1 and S34 and S35). The succinimidate complex **I4** is structurally similar to the dimeric palladacycles with tosylate- and acetate-bridging ligands, **I2** and **I3**, respectively (Fig. 1).

Bromination of L.

The mechanism of Pd^{II}-catalyzed bromination of **L** was studied in the solid state by *in situ* Raman spectroscopy, in particular to establish whether the palladacyclic compounds **I1**-**I4** are formed during the reaction. Bromination of **L** was carried out with 30 or 40 mol% of $Pd(OAc)_2$ or $Pd(OTs)_2(MeCN)_2$ and 0.5 equiv. of TsOH under LAG conditions with 15 μL of MeCN.

Since the possible intermediates **I1**-**I4** have different Raman spectra, we expected that *in situ* Raman monitoring would reveal which of them is the intermediate in this reaction. Indeed, the presence of **I1** as one of the intermediates was confirmed by the appearance of its ν(N=N) band at about 1395 cm^{-1} after 15 min of milling (Fig. 2 and Fig. S25 and S28).

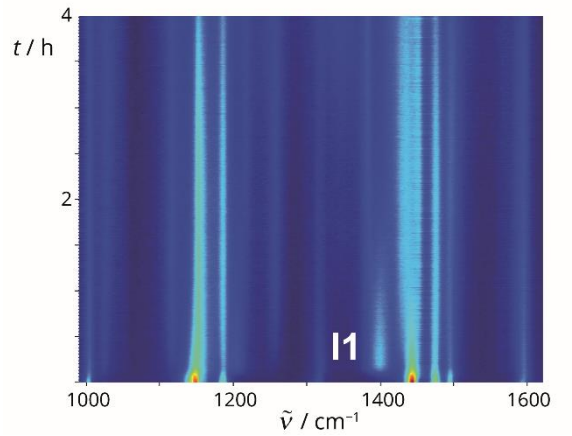

Fig. 2 *In situ* observation of **I1** during the time-resolved Raman monitoring of LAG of **L** (0.50 mmol) with NBS (0.6 mmol), TsOH (0.25 mmol), $Pd(OAc)_2$ (40 mol%.) and MeCN (15 μL).

To our knowledge, this is the first *in situ* observation of the palladacyclic intermediate during a solid-state halogenation reaction. Raman monitoring revealed stepwise reaction dynamics, starting with the formation of **I1**, followed by its conversion to **LBr-I**. (Fig. 2 and S6-S9). The decrease in the intensity of the band at 1395 cm^{-1} was accompanied by the increase in the intensity of the bands at 1476, 1451, 1422 and 1185, 1151, 1116 cm^{-1} assigned to the stretching vibrations of the N=N and C–N bonds of **LBr-I**, respectively. At the same time, an additional band of low intensity was observed at 1382 cm^{-1} with the temporal profile of **LBr-I**. This band was attributed to the stretching vibration of the N=N bond of **I4**, as supported by the Raman spectrum of isolated **I4**, which is possibly formed by the side reaction of succinimidates released during the bromination of **L** by NBS (Fig. S27 and S28). The concentrations of intermediates **I1** and **I4** were too low in all reactions to be reliably quantified in the reaction profiles (Fig. 2 and S6-S9). The presence of palladacyclic intermediates could not be detected in the Raman spectra when the amount of Pd^{II} catalyst was less than 30 mol%, due to the low intensity of the characteristic **I1** bands compared to the Raman bands of the reactant and product. Analogous bromination reactions of **L** with 30 or 40 mol% of $Pd(OAc)_2$ under neat grinding (NG) conditions (without MeCN) also gave **LBr-I**, which could only be confirmed by NMR spectroscopy. The strong fluorescence of the expected dimeric intermediate prevented a more detailed insight into the reactions by Raman spectroscopy. (Fig. S10).

Moreover, we found that all prepared palladacycles **I1-I4** catalyzed the bromination of **L**, which supports their possible participation in the catalytic cycle.[6e] These reactions were carried out with 5 mol% of **I1** or 2.5 mol% of dimeric palladacycles (**I2**, **I3,** and **I4**) as catalysts, **L** (1 equiv.), NBS (1.2 equiv.), TsOH (0.5 equiv.), and MeCN (15 μL) (Fig. 3c and S12-S16). The reaction profiles showed that the conversion rates of **L** to **LBr-I** in the presence of **I1-I4** as catalysts were comparable to those of the analogous reactions using $Pd(OAc)_2$ or $Pd(OTs)_2(MeCN)_2$ as (pre)catalysts (Fig. 3 and S12-S16).

To gain further support for the relevance of palladacycles in the bromination of **L**, we subjected **I1**-**I4** to the NG reactions with 1.2 equiv. (for the monomeric species) and 2.4 equiv. (for the dimeric species) of NBS. In the case of **I1** and **I2**, the NMR spectra of the crude reaction mixtures after 30 min of milling contained the signals of both **LBr-I** and the starting palladacycle, in a molar ratio of about 1:1, and there were no further changes in the NMR spectra with prolonged reaction time (Figs S2 and S3). The addition of 1 equiv. of **L** to the reactions of **I1** and **I2** with NBS resulted in a complete conversion of **I1** to **LBr-I** after 1 h of milling, as confirmed by the NMR spectrum of the crude reaction mixture. *Ex situ* NMR monitoring of the NG reactions of **I3** and **I4** with 2.4 equiv. of NBS revealed complete conversion of the initial palladacycles to **LBr-I** after 3 and 20 h of milling, respectively (Fig. S4 and S5). These results corroborate the possibility that all palladacycles **I1**-**I4** could be part of the catalytic cycle.

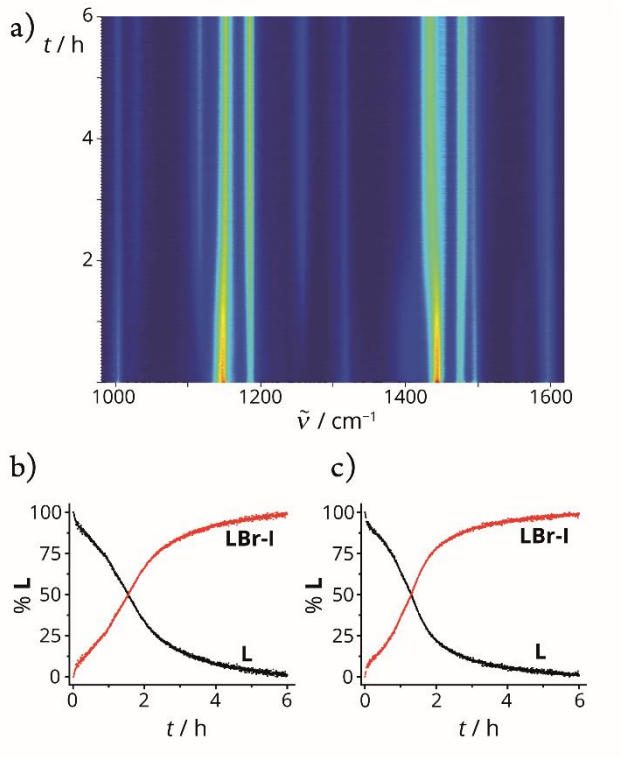

Fig. 3 a) 2D plot of the time-resolved Raman monitoring of LAG of **L** (0.50 mmol) with NBS (0.6 mmol), $Pd(OAc)_2$ (0.025 mmol), TsOH (0.25 mmol) and MeCN (15 μL). Reaction profiles derived from multivariate curve analysis - alternating least squares fitting (MCR-ALS) for the bromination of **L** under LAG conditions using b) $Pd(OAc)_2$ (5 mol%) as a catalyst, and c) **I1** (5 mol%) as a catalyst.

In the Raman spectra of all reaction mixtures containing TsOH, the low intensity band at 1403 cm^{-1} was detected in the early phase. This band was assigned to the N=N bond stretching of the protonated **L**, which was confirmed by Raman monitoring of the reaction of **L** with TsOH.[19] In addition to **L**, TsOH could also protonate NBS, which could have significant influence on the bromination mechanism.[20]

C–H bond activation.

To gain a complete insight into the nature and reactivity of the observed and expected palladacyclic intermediates under mechanochemical conditions, the formation of tosylate palladacycles from **L** and $Pd(OTs)_2(MeCN)_2$ or a mixture of $Pd(OAc)_2$ and TsOH, with or without the addition of MeCN, was monitored by Raman spectroscopy.

NG and LAG of $Pd(OTs)_2(MeCN)_2$ and **L** in a molar ratio of 1:1 gave the monomeric monopalladated species **I1**, which was detected by NMR spectroscopy (Fig. S42-S46). The molecular structure of **I1**, resolved from PXRD data, confirmed that the palladium center is coordinated by the azo nitrogen atom and the carbon atom of the phenyl ring of azobenzene, the nitrogen atom of MeCN, and the oxygen atom of tosylate, which is in *trans* position to the Pd–C bond (Fig. 1 and S32). *In situ* Raman monitoring of both reactions confirmed the complete conversion of **L** to **I1** after 90 min of milling (Fig. 4). This conversion resulted in a large shift of the ν(N=N) bands at 1493, 1472, 1442 cm^{-1} in **L** to 1395 cm^{-1} in **I1** and a decrease and shift of the ν(C–N) band at 1147 cm^{-1} in **L** to 1207 cm^{-1} in **I1** (Fig. 4 and S17). The reaction profiles showed that there was no difference in the rates of C–H bond activation with $Pd(OTs)_2(MeCN)_2$ in NG and LAG reactions. In contrast to MeCN used as an additive in the LAG reaction, the addition of 1 equiv. of TsOH to a mixture of $Pd(OTs)_2(MeCN)_2$ and **L** accelerates C–H bond activation (Fig. S18). This result suggests that TsOH could promote proton transfer from the phenyl ring of **L** to the tosylate ligand. Further increasing the amount of TsOH slowed down the reactions (Fig. S19). In the Raman spectra of all reactions with $Pd(OTs)_2(MeCN)_2$ and **L**, a small shift in the ν(C–N) and ν(N=N) bands of **L** was observed after three minutes of milling. The observed changes were attributed to the formation of the intermediate adduct, in which the intramolecular C–H bond activation takes place.[21]

LAG of $Pd(OAc)_2$ with **L** and TsOH, using 25 μL of MeCN as an additive, in a molar ratio of 1:1:1 (**L**:$Pd(OAc)_2$:TsOH) or 1:1:2 (**L**:$Pd(OAc)_2$:TsOH) also gave the monopalladated product **I1** (S33). Monitoring of these reactions by Raman spectroscopy corroborated the analogous reaction course as for the reaction with $Pd(OTs)_2(MeCN)_2$ (Fig. 4 and S20), indicating the *in situ* formation of a mono- or bistosylate species, $Pd(OTs)(OAc)(MeCN)_2$ or $Pd(OTs)_2(MeCN)_2$, from $Pd(OAc)_2$.[17b,c] The reaction times required for the complete conversion of **L** and $Pd(OAc)_2$ to **I1** are slightly longer than for the reaction with $Pd(OTs)_2(MeCN)_2$, indicating rapid *in situ* formation of the tosylate species by breaking up the acetate trimer with TsOH and MeCN. The substitution of acetate by tosylate was accompanied by the release of acetic acid as a byproduct and the binding of MeCN to the metal center. The reaction profiles showed that the addition of 2 equiv. of TsOH to a mixture of $Pd(OAc)_2$ and **L** accelerated the C–H bond activation (Fig. S21). The formation of **I1** in both reactions of $Pd(OAc)_2$ with **L** was accompanied by the characteristic increase in the intensity of the ν(N=N) and ν(C–N) bands at about 1395 cm^{-1} and 1207 cm^{-1}, respectively (Fig. S20 and S21). In addition to the Raman spectra, the formation of **I1** was also confirmed by NMR spectroscopy and PXRD (Fig. S42-S46 and S32).

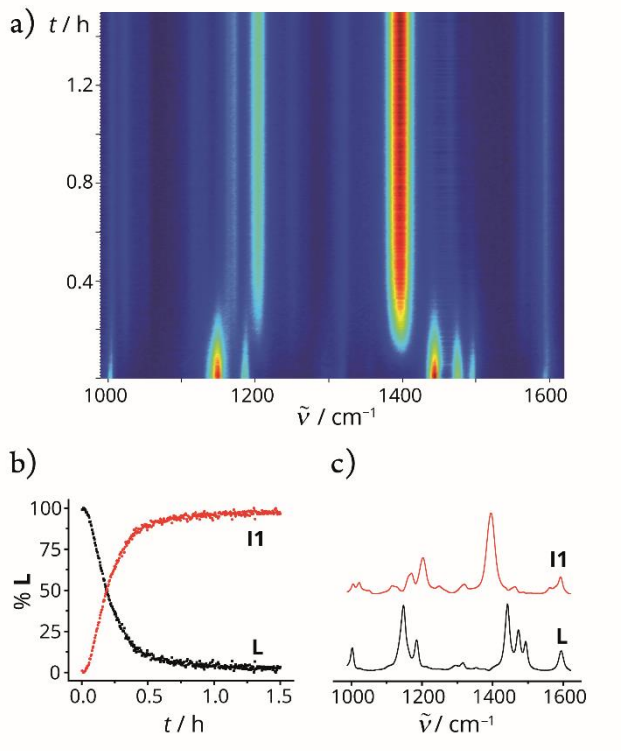

Fig. 4 a) 2D plot of the time-resolved Raman monitoring of LAG of **L** (0.40 mmol) with $Pd(OTs)_2(MeCN)_2$ (0.42 mmol) and MeCN (0.48 mmol, 25 µL). b) Reaction profile derived from MCR-ALS fitting. c) Extracted Raman spectra of species observed during Raman monitoring.

On the other hand, C–H bond activation reactions performed in the absence of MeCN showed a different reaction course and resulted in a different product than those performed in the presence of MeCN (Fig. 5 and S22). NG of $Pd(OAc)_2$ with **L** and TsOH in a molar ratio of 1:1:1 (**L**:$Pd(OAc)_2$:TsOH) led to the monopalladated product **I2** after 3 h of milling. The molecular structure of the isolated product **I2**, solved by PXRD, revealed that **I2** is a dimer with *transoid* geometry in which the two monocyclopalladated azobenzene moieties are bridged by two tosylate ligands in an open-book arrangement (Fig. 1 and S33). The aromatic region of the ^{1}H NMR spectrum of **I2**, recorded in DMSO-d_6 was similar to that of **I1**, suggesting that **I2** is converted to the monomeric species by cleavage of the tosylate bridges with the strong donor solvent DMSO-d_6 (Fig. S48). *In situ* Raman monitoring revealed that the rapid decrease in the intensity of the **L** bands coincided with the increase in the intensity of the ν(N=N) and ν(C–N) bands at 1396 cm^{-1} and 1203 cm^{-1}, respectively. Based on their positions and in comparison with reactions in which **I1** is formed, we assigned them to the monomeric monopalladated species with bidentate bound tosylate or with terminal tosylate and H_2O as ancillary ligands. H_2O was introduced into the reaction mixture with TsOH in the monohydrate form. The band intensities at 1396 cm^{-1} and 1203 cm^{-1} decreased after 10 min of milling and new bands appeared at 1384 and 1303 cm^{-1}, which could correspond to **I2** (Fig. 5 and S22 and S23). This result suggests that the dimerization process occurs after cyclopalladation. Unfortunately, reliable assignment of the **I2** bands was not possible because the Raman spectrum of the isolated dimer **I2** could not be obtained due to its strong fluorescence.

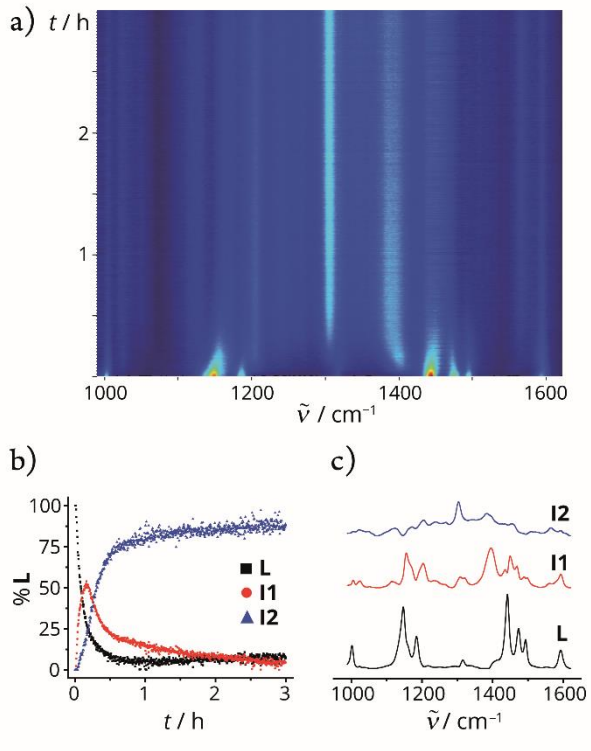

Fig. 5 a) 2D plot of the time-resolved Raman monitoring of NG of **L** (0.40 mmol) with $Pd(OAc)_2$ (0.42 mmol) and TsOH (0.42 mmol). b) Reaction profile derived from MCR-ALS analysis. c) Extracted Raman spectra of species observed during Raman monitoring.

In situ Raman monitoring of the C–H bond activation of **L** provided additional evidence that halogenation of **L** under mechanochemical conditions occurs via monomeric or dimeric palladacycles as intermediates, with the monomeric route being more efficient providing a higher yield and a faster reaction rate.

DFT calculations.

The computational setup is given in Section 8 of the ESI. The presented cyclopalladation and the bromination reactions take place in the solid state, but the mechanism was modelled as in the vacuum, because no appropriate parameters for the polarizable continuum (PCM)[22] or a model alike, are available. It was recently demonstrated[23] that PCM can be relatively simply extended to solid state reactions, by using the weighted combinations of the medium constituent parameters. However, in the present case the relevant parameters (dielectric constant, refractive index) for the substances involved are not available. We assume that the functional mechanism in the vacuum would also work in the solid state, only faster due to increased concentrations and greater medium polarizability.[23] In other words, the medium influence is supposed to affect only the energy values, without inducing a specific solid state pathway. Hence, the mechanistic pathway determined for vacuum should provide a qualitative insight into the solid state mechanism as well. The reaction steps with charge separation and possibly critical medium effect, were also examined by using PCM with MeCN as the solvent. MeCN was chosen because it is present in the LAG reactions (although far from a typical solvent concentration), and because it is moderately polar and aprotic solvent with mild solvation effect, thus suitable for a reserved estimation of the unknown medium influence.

The mechanism was modelled starting from free NBS and **I1** as the reactants. Our experimental results and some others[16] confirm that in the presence of MeCN the reaction takes place from **I1**. It does not preclude another pathway, from dimeric form **I2**, which is also supported by experimental results[24] including those presented here. However, the size of **I2** and the multiplicity of mechanistic variants make modelling from **I2** much more complex. The mechanism operative with **I1** should be applicable to **I2**, with necessary modifications. The reverse extension from **I2** to **I1** may not hold, due to a potentially specific influence of the interaction between two palladium atoms in **I2**. Therefore, the redox steps were additionally checked by computations involving the appropriate dimeric forms, but no such influence was indicated in the results

I1 may assume a number of conformations due to many possible orientations of tosylate bound to the palladium atom. Among several examined conformations, the one with the least free energy was chosen for the modelling. There is no indication that different conformations could lead to significantly different reaction profiles. We would like to emphasize that the relative energies of the stationary points were calculated in respect to the coordinatively saturated palladium species, in contrast to some customized approaches where the initial species are in activated form (coordinatively unsaturated or with less efficient bidentate coordination of e.g. acetate or tosylate ions). The reaction barriers from activated reference species may appear lower than they really are.

The bromination mechanism was basically considered in terms of the bromine donor species and of the acceptor atom in **I1**. It is known that NBS requires some kind of activation to be an efficient donor, and the acidic medium is one of such promotors.[6k,25] As our experimental results indicate that presence of a strong acid is beneficial, we have examined bromine transfer from three possible sources (i) NBS alone, (ii) the complex NBS···*p*-TsOH

formed by hydrogen bond between the oxygen atom of NBS and the acidic proton of *p*-TsOH, and (iii) the protonated NBS ($NBSH^+$) with proton on the oxygen atom (as the most stable isomer). In regard to the bromine atom acceptor, two possibilities arise: (a) transfer to the palladium atom and the subsequent 1,2-shift to the carbon atom, and (b) direct transfer to the carbon atom. The pathway (a) is commonly designated as the oxidative addition + reductive elimination (OA+RE), and (b) is termed the electrophilic cleavage (EC) since formation of the C–Br bond occurs simultaneously with breaking of the Pd–C bond.[26]

Attempts to achieve a direct transfer of bromine atom from NBS to palladium atom in **I1** were unsuccessful. When the distance between Pd and Br was shortened, the energy would only increase, with no indication the N–Br bond breaking and the Pd–Br bond formation. The same result was obtained with the complex NBS···*p*-TsOH instead of NBS. Since the attempted reaction step involves charge separation, we repeated these scans with PCM and MeCN as the solvent, and the results were the same, as well as with the dimer **I2** instead of **I1**. We concluded that the oxidative addition with free electroneutral brominating agent is not possible. However, if NBS had been first introduced into the coordination sphere of Pd atom (with oxygen as the ligating atom) by substitution of MeCN, the bromine transfer became possible. Hence, we introduced the ligand substitution (LS) as the initial step in the OA+RE pathway. On the other hand, the bromine transfer from free NBS or NBS···*p*-TsOH to the activated carbon atom of **I1** went smoothly, through a single transition state, with bromine atom halfway between the nitrogen and carbon atoms, at the distance of 2.22 Å from each, and with assistance of the palladium atom at 2.58 Å from bromine. In contrast to these findings, the bromine transfer from $NBSH^+$ to palladium atom was spontaneous, with no barrier at all. A similar transfer to the activated carbon atom was not possible, because the transfer to the adjacent palladium atom was much more competitive. Based on these preliminary results we anticipated reaction mechanisms sketched in Scheme 1. By calculating all the stationary points implied, we obtained the free energy profiles of the pathways **I-III** shown in Fig. 6 and 7.

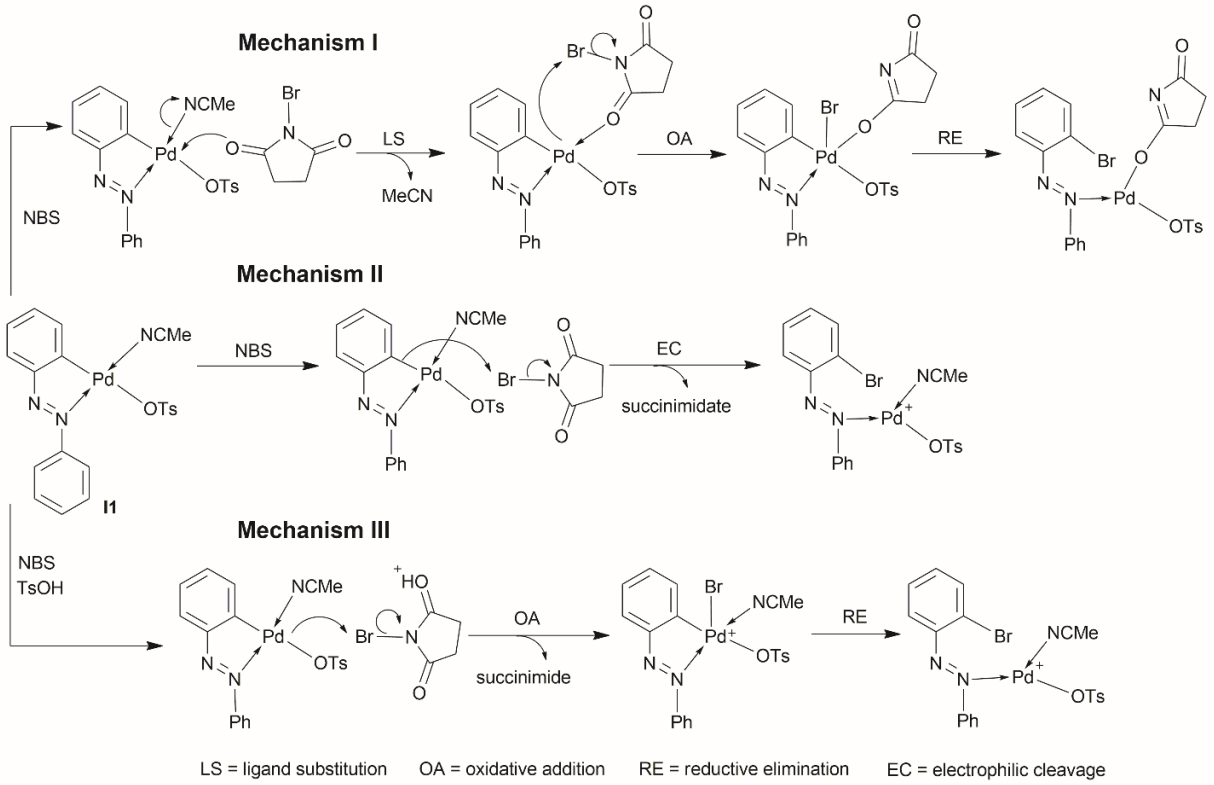

Scheme 1 The considered mechanistic pathways. The mechanisms **I** and **II** are shown with NBS as the active bromination species; a similar pathway with the hydrogen bond complex NBS···*p*-TsOH instead of NBS was also considered.

High energy barriers in the OA step of the mechanisms **I** and **II** (Fig. 6), with either NBS or NBS···*p*-TsOH as the bromination species, prompted us to examine a possibility of the radical mechanism. To this end we checked whether the energy of the ts(OA) geometry would be lower if unrestricted wavefunction was used. Indeed, the single point DFT calculation resulted in the singlet biradical state with a significantly lower energy. Reoptimization of ts(OA) with the unrestricted (broken symmetry) DFT ended up in the local minimum i(OA) (Fig. 6) instead in the transition state. The subsequent scans from i(OA) towards the reactant and the product geometries, performed by shortening N–Br and Pd–Br distances, respectively, revealed two new transition states, ts1(OA) and ts2(OA). After a few steps along the intrinsic reaction coordinates (IRC) from ts1(OA) to the reactant r(OA), and from ts2(OA) to the product p(OA), the biradical singlet wavefunction collapses into a common closed shell singlet. Hence, the biradical singlet character is limited to a relatively narrow region around ts1(OA) and ts2(OA) and in between them. This region is characterized by the greater stability of the triplet state compared to the closed shell singlet (Table 2). At i(OA) the triplet state is even more stable (slightly) than the biradical singlet. The geometries of ts1(OA), i(OA) and ts2(OA) are very similar (Fig S54). The occurrence of i(OA) is probably an artifact of the broken symmetry DFT method; with proper multiconfigurational method the stationary points ts1(OA), i(OA) and ts2(OA) would possibly merge into a single transition state. Biradical singlet character was confirmed by the single point CAS(2,2) calculations. The occupancies of the two active orbitals

are: (1.9, 0.1), (1.2, 0.8) and (1.5, 0.5) for ts1(OA), i(OA) and ts2(OA), respectively. After Boys localization,[27] the two active orbitals are very similar to the two semioccupied orbitals of the triplet state, in parallel with the DFT spin density distribution (Fig. S55).

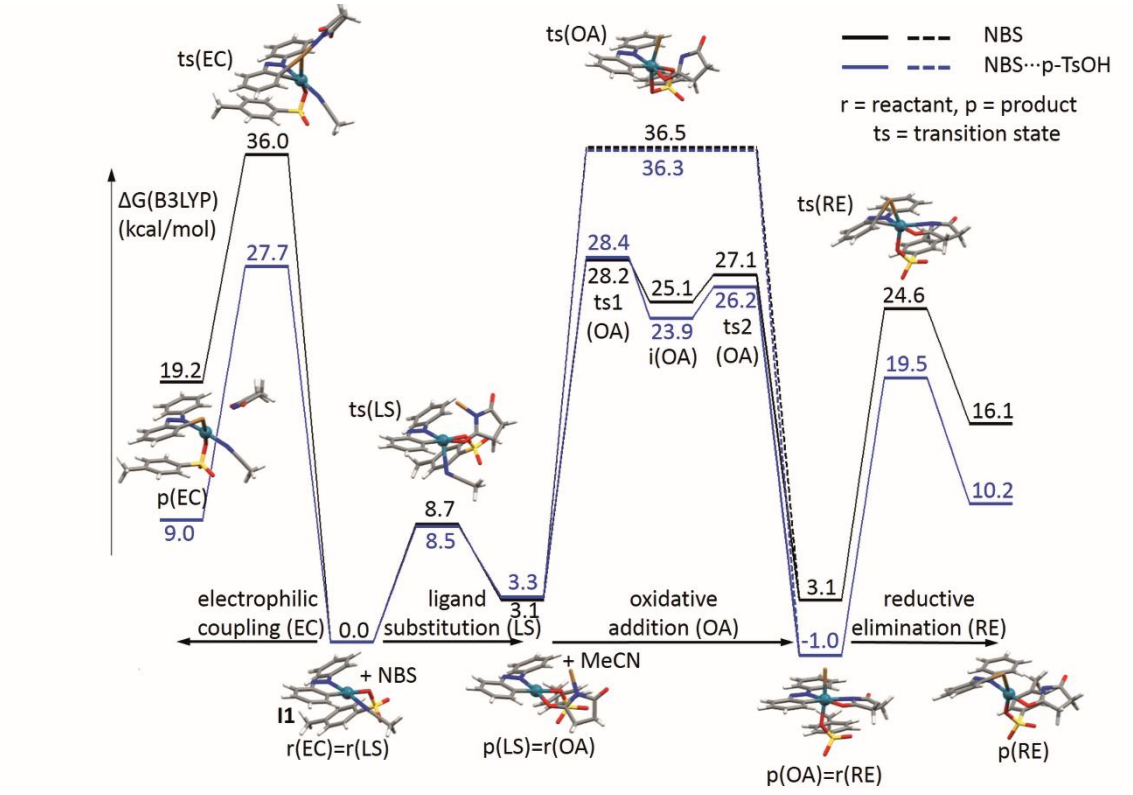

Fig. 6 Free energy profile of the bromination of **I1**; mechanism **I**: ligand substitution followed by oxidative addition and reductive elimination (on the right side of **I1**+NBS), and mechanism **II**: by electrophilic coupling (on the left side of **I1**+NBS). The relative free energies are given in kcal/mol (B3LYP/def2TZVP). The geometries shown are from the closed shell singlet calculations with NBS as the brominating species.

Table 2 Closed shell singlet and triplet energies for the geometries in the OA step, relative to the singlet biradical (B3LYP/def2TZVP, in kcal/mol)

	Closed Shell Singlet	Triplet
ts1(OA)	3.5	2.7
i(OA)	11.7	−0.3
ts2(OA)	2.6	2.1

After biradical singlet transition state was found in the OA step, stability of the closed shell singlet wavefunctions was checked for all other transition states, and the closed shell wavefunction was confirmed as stable in all cases. The check was extended to the geometries from a scan of the bromine transfer directly from free NBS to palladium in **I1**, and the same (negative) result was obtained.

The halogenation products p(EC) and p(RE) (Fig. 6) are not the final and the most stable forms. For example, p(EC) may easily rearrange into another configuration (Fig. S56) which is 18.9 kcal/mol more stable than **I1**+NBS. Hence the reaction is predicted to be exergonic.

The hydrogen bond complex NBS···*p*-TsOH was considered as another bromination species because the donation of Br^+ could be eventually promoted by the hydrogen bond or perhaps even by the concerted proton transfer from *p*-TsOH to NBS. This would also explain the beneficial influence of *p*-TsOH on the bromination yield. The complex seems to have some effect in the EC and RE steps, while the barriers in the OA step remain much the same. This could be because in OA step NBS is ligated to the positively charged palladium atom, hence the proton close to the other oxygen atom of NBS does not make a difference. The barrier lowering in RE step by 5.1 kcal/mol can be related to more intense dispersive interactions between the hydrogen bonded *p*-TsOH and the other molecular fragments. Namely, after the OA step, geometrical relaxation brings *p*-TsOH closer to the tosylate anion and ends by their alignment with azobenzene. A similar effect was noticed also in the EC step whose barrier is lower by 8.3 kcal/mol. However, here the hydrogen bond also contributes because in the alternative transition state configuration, with *p*-TsOH bound to the oxygen atom of NBS which is more distant from the rest of the molecular assembly, the barrier is also lower, but by only 4.3 kcal/mol (Fig. S57).

As a conclusion, the mechanisms **I** (either with NBS or NBS···*p*-TsOH) with singlet biradical transition states, and **II** with NBS···*p*-TsOH, appear comparably operative, with barriers in the rate determining steps at about 28 kcal/mol. Although this value is relatively high, it is reasonable to expect that in the solid-state medium these barriers could be remarkably lower.

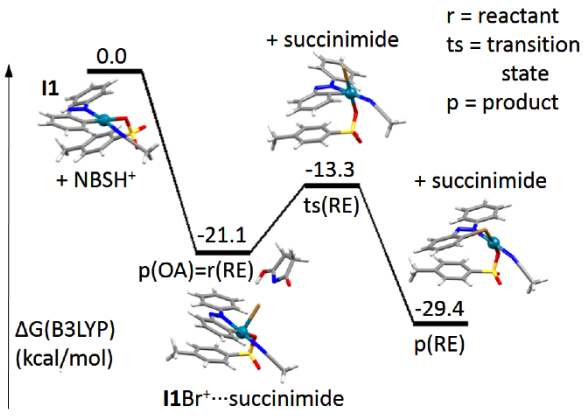

Fig. 7 Free energy profile of the bromination of **I1** by the mechanism **III**.

The pathway with $NBSH^+$ as the active bromination species (mechanism **III**) is particularly attractive because Br^+ migrates to palladium atom spontaneously, with no energy barrier. The free energy of the complex **I1**$Br^+\cdots$succinimide is 21.1 kcal/mol below the separate pair of $NBSH^+$ and **I1**. In the subsequent RE step the barrier is only 7.8 kcal/mol above **I1**Br^+, which all together makes the mechanism **III** quite favorable. However, there remains the question whether NBS can be protonated by *p*-TsOH, as it was tacitly assumed by now. The energy of the ionized pair ($NBSH^+$ and *p*-TsO^-) is 121.2 kcal/mol (in vacuum) above the energy of the neutral pair (NBS and *p*-TsOH), which makes protonation of NBS rather unlikely. However, when this difference is calculated for the solution (in MeCN, B3LYP/def2TZVP/SMD), it drops to only 20.2 kcal/mol. This value is still too high for a significant extent of protonation, but the influence of the solid-state medium could be much stronger than of MeCN, and there is also the uncertainty of the calculation method of about 4 kcal/mol for ions.[28]

As the final conclusion, none of the three considered mechanistic pathways can be abandoned on the basis of the experimental results and the current level of computational modelling. Even all three could be operative with their relative participations depending on the reaction conditions. Positive effect of *p*-TsOH on the bromination yields can be associated with NBS$\cdots$*p*-TsOH as the active bromination agent in pathways **I** or **II**, or with the protonated NBS in the pathway **III**. However, bromination in the stoichiometric mixture of NBS and **I1**, **I2**, **I3** or **I4**, which proceeds without addition of *p*-TsOH, is best explained by the pathway **I** with NBS.

The cyclopalladation mechanism has been modelled according to the previously reported results for the azobenzene ligand.[29] The reported mechanism with $PdCl_2$ in DMF involves two steps; first, formation of the agostic complex with the coordinating DMF molecule displaced by the activating C–H bond, and second, the hydrogen transfer from C–H bond to the oxygen atom of the displaced DMF. A similar mechanism was assumed in the present case, starting with the adduct in which Pd is coordinated by azobenzene, two tosylate anions and MeCN. However, the agostic intermediate could not be obtained as the minimum point. It was found only if one tosylate anion was completely removed. Only the hydrogen transfer transition state was obtained, at 20.3 kcal/mol (vacuum). The intrinsic reaction coordinate toward the reactant ends up with the geometry of the agostic intermediate but the subsequent optimization (with small maximum step size) slowly converges to the reactant adduct, not to the agostic intermediate. This should not be surprising because the agostic intermediate necessitates charge separation which is not stable in the vacuum.

Conclusion

In the presented work, we have gained a direct insight into the course of regioselective mechanochemical Pd^{II}-catalyzed halogenation of the C–H bond in azobenzene using a combination of *in situ* reaction monitoring by Raman spectroscopy and DFT calculations. Reaction profiles showed that the halogenation of azobenzene is a multistep process in which catalytically active Pd^{II} species are formed *in situ* from *p*-TsOH and $Pd(OAc)_2$, followed by the formation of a monomeric or dimeric palladacyclic intermediates, that then react with NXS to form the final orthohalogenated product. The nature of the active Pd^{II} catalysts and the palladacyclic intermediates depends on the presence or absence of MeCN as a liquid additive in the reaction mixture. Moreover, *in situ* Raman monitoring revealed that *p*-TsOH activates NXS and affects the rates of C–H bond activation.

Quantum-chemical modelling revealed three possible reaction mechanism pathways for bromination of cyclopalladated azobenzene. The bromine atom can be transferred first to the palladium atom, by the oxidative addition. It may happen from electroneutral NBS (or the complex NBS···*p*-TsOH) only if NBS is one of the ligands in the Pd-coordination shell. With protonated NBS, this is not necessary, and the migration of Br^+ goes directly from free $NBSH^+$, in a barrierless process. The bromine atom shifts to the carbon atom in the subsequent reductive elimination step. In the alternative, electrophilic cleavage pathway, the carbon atom is brominated directly from free NBS (or NBS···*p*-TsOH), with simultaneous breaking of the Pd–C bond. The transition state in the oxidative addition with electroneutral species is characterized by the singlet biradical electronic structure. The barriers in the electroneutral pathways are similar, at around 28 kcal/mol (vacuum). With $NBSH^+$ as the bromine source, the mechanism efficiency is governed by the protonation extent, which is at a quite detectable level, as indicated experimentally. These results expand the scope of catalytic C–H halogenation in the solvent-free and environmentally friendly reaction conditions, which is consistent with the main goals of green chemistry. Moreover, the understanding of the reaction dynamics provided by the *in situ* Raman monitoring data and DFT calculations will also enable a better design and control of Pd-catalyzed C–H bond functionalization by mechanochemistry.

Conflicts of interest

There are no conflicts to declare.

Acknowledgements

Financial support was provided by Croatian Science Foundation (grant No. IP-2019-04-9951). Computations were done on the Isabella cluster at SRCE, Zagreb, Croatia. We thank Dr José G. Hernández (Ruđer Bošković Institute) for critically reading the manuscript.

References

1. R. C. Larock, *Comprehensive Organic Transformations*, Ed. Wiley-VCH, Weinheim, 1999; pp 609–666; (b) J. March, *Advanced Organic Chemistry*, Wiley, New York, 1992, pp 531–534 and 689–694; (c) *Chemistry of the Carbon–Halogen Bond*, (Ed.: S. Patai) Wiley, New York, 1973; (d) C. L Raston and G. Salem, *Chemistry of the Metal–Carbon Bond*, (Ed.: F. R. Hartley) Wiley, Chichester (UK), 1987, **4**, pp 159–306.
2. D. A. Petrone, Y. Ye and M. Lautens, Modern transition-metal-catalyzed carbon–halogen bond formation, *Chem. Rev*. 2016, **116**, 8003–8104.
3. (a) S. Rohrbach, A. J. Smith, J. H. Pang, D. L. Pool, T. Tuttle, S. Chiba and J. A. Murphy, Concerted nucleophilic aromatic substitution reactions, *Angew. Chem. Int. Ed*. 2019, **58**, 16368–16388; (b) F. Terrier, *Modern Nucleophilic Aromatic Substitution*, Wiley-VCH, Weinheim, 2013.
4. (a) G. S. Silverman and P. E. Rakita, *Handbook of Grignard Reagents*, (Eds.: M. Dekker), New York, 1996; (b) N. Sotomayor and E. Lete, Aryl and heteroaryllithium compounds by metal–halogen exchange, *Curr. Org. Chem.* 2003, **7**, 275–300.
5. L. Nattman, R. Saeb, N. Nöthling and J. Cornella, An air-stable binary Ni(0)–olefin catalyst. *Nat. Catal*. 2020, **3**, 6–13; (b) J. I. Ayogu and A. E. Onoabdedje, Recent advances in transition metal–catalysed cross-coupling of (hetero)aryl halides and analogues under ligand-free conditions, *Catal. Sci. Technol*. 2019, **9**, 5233–5255; (c) Y. Zhai, X. Chen, W. Zhou, M. Fan, Y. Lai and D. Ma, Copper-catalyzed diaryl ether formation from (hetero)aryl halides at low catalytic loadings *J. Org. Chem.* 2017, **82**, 4964–4969; (d) J. F. Hartwig, *Handbook of Organopalladium Chemistry for Organic Synthesis*, (Ed.: E. Negish(i), Wiley-Interscience, New York, 2002, pp 1051–1096 and 1097–1106; (e) J. K. Stille, The palladium-catalyzed cross-coupling reactions of organotin reagents with organic electrophiles [New synthetic methods (58)], *Angew. Chem. Int. Ed. Engl*. 1986, 25, 508–524; (f) R. F. Heck, Cobalt and palladium reagents in organic synthesis: The beginning, *Synlett* 2006, 2855–2860; (g) A. Suzuki, Carbon–carbon bonding made easy, *Chem. Commun*. 2005, 4759–4763; (h) A. R. Muci and S. L. Buchwald, Practical palladium catalysts for C–N and C–O bond formation, *Top. Curr. Chem*. 2002, 219, 131–209; (i) J. F. Hartwig, Discovery and understanding of transition-metal-catalyzed aromatic substitution reactions, *Synlett* 2006, 1283–1294; (j) J. F. Hartwig, Carbon–heteroatom bond formation catalysed by organometallic complexes, *Nature* 2008, **455**, 314–322; (k) Z.-S. Gu, W.-X. Chen and L.-X. Shao, *N*-heterocyclic carbene-palladium(II)-1-methylimidazole complex-catalyzed direct C–H bond arylation of (benz)imidazoles with aryl chlorides, *J. Org. Chem*. 2014, **79**, 5806–5811.
6. (a) L. Wang and B. P. Carrow, Electrophilic concerted metalation-deprotonation (eCMD), *ACS Catal*. 2019, **9**, 6821–6836; (b) S. Qian, Z.-Q. Li, M. Li, S. R. Wisniewski, J. X. Qiao, J. M. Richter, W. R. Ewing, M. D. Eastgate, J. S. Chen and J.-Q. Yu, Ligand-enabled Pd(II)-catalyzed C(sp^3)–H lactonization using molecular oxygen as oxidant, *Org. Lett*. 2020, **22**, 3960−3963; (c) X.-H. Liu, H. Park, J.-H. Hu, Y. Hu, Q.-L. Zhang, B.-L. Wang, B. Sun, K.-S. Yeung, F.-L. Zhang and J.-Q. Yu, Diverse ortho-C(sp^2)–H functionalization of benzaldehydes using transient directing groups, *J. Am.*

Chem. Soc. 2017, **139**, 888–896; (d) P. C. Powers and T. Ritter, Bimetallic Pd(III) complexes in palladium-catalysed carbon–heteroatom bond formation, *Nat. Chem*. 2009, **1**, 302–309; (e) A. R. Dick, K. L. Hull and M. S. Sanford, A highly selective catalytic method for the oxidative functionalization of C−H bonds, *J. Am. Chem. Soc*. 2004, **126**, 2300–2301; (f) R. Giri, X. Chen and J.-Q. Yu, Palladium-catalyzed asymmetric iodination of unactivated C–H bonds under mild conditions, *Angew. Chem. Int. Ed*. 2005, **44**, 2112–2115; (g) R. Giri, X. Chen, X.-S. Hao, J.-J. Li, J. Liang, Z.-P. Fan and J.-Q. Yu, Catalytic and stereoselective iodination of prochiral C–H bonds, *Tetrahedron: Asymmetry* 2005, **16**, 3502–3505; (h) K. L. Hull, W. Q. Anani and M. S. Sanford, Palladium-catalyzed fluorination of carbon-hydrogen bonds, *J. Am. Chem. Soc*. 2006, **128**, 7134–7135; (i) D. Kalyani, A. R. Dick, W. Q. Anani and M. S. Sanford, Scope and selectivity in palladium-catalyzed directed C–H bond halogenation reactions, *Tetrahedron* 2006, **62**, 11483–11498; (j) D. Kalyani, D.; A. R. Dick, W. Q. Anani and M. S. Sanford, A simple catalytic method for the regioselective halogenation of arenes, *Org. Lett*. 2006, **8**, 2523–2526; (k) R. B. Bedford, M. F. Haddow, C. J. Mitchell and R: L. Webster, Mild C–H halogenation of anilides and the isolation of an unusual palladium(I)–palladium(II) species, *Angew. Chem. Int. Ed*. 2011, **50**, 5524–5527; (l) J. J. Topczewski, P. J. Cabrera, N. I. Saper and M. S. Sanford, Palladium-catalysed transannular C–H functionalization of alicyclic amines, *Nature* 2016, **531**, 220–224; (m) T. W. Lyons and M. S. Sanford, Palladium-catalyzed ligand-directed C−H functionalization reactions, *Chem, Rev*. 2010, **110**, 1147–1169; (n) A. McNally, B. Haffemayer, B. S. L. Collins and M. J. Gaunt, Palladium-catalysed C–H activation of aliphatic amines to give strained nitrogen heterocycles, *Nature* 2014, **510**, 129–133; (o) J. Yamaguchi, A. D. Yamaguchi and A. K. Itami, C–H bond functionalization: emerging synthetic tools for natural products and pharmaceuticals, *Angew. Chem. Int. Ed*. 2012, **51**, 8960–9009; (p) L. Ackermann, Carboxylate-assisted transition-metal-catalyzed C−H bond functionalizations: mechanism and scope, *Chem. Rev*. 2011, **111**, 1315; (q) K. Godula and D. Sames, C-H Bond Functionalization in Complex Organic Synthesis, *Science* 2006, **312**, 67–72.

7. (a) P. B. D. De la Mare, *Electrophilic Halogenation*, Cambridge University Press, New York, 1976; (b) H. H. Hodgson, The Sandmeyer reaction, *Chem. Rev.* 1947, **40**, 251–277.
8. (a) S. Nakamatsu, S. Toyota, W. Jones and F. G. Toda, The important role of solvent vapour in an organic solid-state reaction, *Chem. Commun.* 2005, 3808–3810; (b) M. J. Cliffe, C. Mottillo, D. K. Bučar and T. Friščić, Accelerated aging: a low-energy, solvent-free alternative to solvothermal and mechanochemical synthesis of metal-organic materials, *Chem. Sci.* 2012, **3**, 2495-2500; (c) M. Juribašić Kulcsár, I. Halasz, A. Budimir, K. Užarević, S. Lukin, A. Monas, F. Emmerling, J. Plavec and M. Ćurić, Reversible gas-solid ammonia N–H bond activation mediated by an organopalladium complex, *Inorg. Chem.* 2017, **56**, 5342–5351. (d) A. Monas, K. Užarević, I. Halasz, M. Juribašić Kulcsár and M. Ćurić, Vapour-induced solid-state C–H bond activation for the clean synthesis of an organopalladium biothiol sensor, *Chem. Commun.* 2016, **52**, 12960–12963.

9. (a) K. J. Ardila-Fierro and J. G. Hernandez, Sustainability assessment of mechanochemistry by using the twelve principles of green chemistry, *ChemSusChem* 2021, **14**, 2145–2162. (b) S. L. James, C. J. Adams, C. Bolm, D. Braga, P. Collier, T. Friščić, F. Grepioni, K. D. M. Harris, G. Hyett, W. Jones, A. Krebs, J. Mack, L. Maini, A. G. Orpen, I. P. Parkin, W. C. Shearouse, J. W. Steed and D. C. Waddell, Mechanochemistry: opportunities for new and cleaner synthesis, *Chem. Soc. Rev.* 2012, **41**, 413–417; (c) T. Friščić, Supramolecular concepts and new techniques in mechanochemistry: cocrystals, cages, rotaxanes, open metal–organic frameworks, *Chem. Soc. Rev.* 2012, **41**, 3493–3510; (d) G.-W. Wang, Mechanochemical organic synthesis, *Chem. Soc. Rev.* 2013, **42**, 7668–7700; (e) D. Braga, L. Maini and F. Grepioni, Mechanochemical preparation of co-crystals, *Chem. Soc. Rev*. 2013, **42**, 7638–7648; (f) N. R. Rightmire and T. P. Hanusa, Advances in organometallic synthesis with mechanochemical methods, *Dalton Trans*. 2016, **45**, 2352–2362; (g) A. R. Sheldon, The E factor 25 years on: the rise of green chemistry and sustainability, *Green Chemistry*, 2017, **19**, 18–43.
10. (a) E. Boldyreva, Mechanochemistry of inorganic and organic systems: what is similar, what is different?, *Chem. Soc. Rev*. 2013, **42**, 7719–7738; (b) V. Šepelak, A. Düvel, M. Wilkening, K. D. Becker and P. Heitjans, Mechanochemical reactions and syntheses of oxides, *Chem. Soc. Rev.* 2013, **42**, 7507–7520; (c) R. Janot and D. Guerard, Nanoparticle technologies: chapter 3. Dry production methods, *Prog. Mater. Sci.* 2005, **50**, 1–92; (d) A. L. Garay, A. Pichon and S. L. James. Solvent-free synthesis of metal complexes, *Chem. Soc. Rev*. 2007, **36**, 846–855.
11. (a) C. Bolm, J. G. Hernandez, From synthesis of amino acids and peptides to enzymatic catalysis: a bottom-up approach in mechanochemistry, *ChemSusChem*, 2018, **11**, 106–110. (b) A. Porcheddu, E. Colacino, L. De Luca and F. Delogu, Metal-mediated and metal-catalyzed reactions under mechanochemical conditions, *ACS Catal*. 2020, **10**, 8344–8394; (c) C. Schumaher, J. G. Hernández and C. Bolm, Electro-mechanochemical atom transfer radical cyclizations using piezoelectric $BaTiO_3$, *Angew. Chem. Int. Ed*. 2020, **59**, 16357–16360; (d) J. G. Hernández and C. Bolm, Altering product selectivity by mechanochemistry, *J. Org. Chem.* 2017, **82**, 4007–4019; (e) J. G. Hernandez, C−H bond functionalization by mechanochemistry, *Chem. Eur. J.* 2017, **23**, 17157–17165; (f) S. Zhao, Y. Li, C. Liu and Y. Zhao, Recent advances in mechanochemical C–H functionalization reactions, *Tetrahedron Lett.* 2018, **59**, 317–324; (g) V. Declerck, P. Nun, J. Martinez and F. Lamaty, Solvent-free synthesis of peptides, *Angew. Chem. Int. Ed.* 2009, **48**, 9318–9321; (h) J. L. Howard, Q. Cao and D. L. Browne, Mechanochemistry as an emerging tool for molecular synthesis: what can it offer?, *Chem. Sci.* 2018, **9**, 3080–3094; (i) J. Andersen and J. Mack, Mechanochemistry and organic synthesis: from mystical to practical, *Green Chem.* 2018, **20**, 1435–1443; (j) A. Stolle, L. Szuppa, S. E. S. Leonhardt and B. Ondruschka, Ball milling in organic synthesis: solutions and challenges, *Chem. Soc. Rev*. 2011, **40**, 2317–2329; (k) J.-L Do, C. Mottillo, D. Tan, V. Štrukil and T. Friščić, Mechanochemical ruthenium-catalyzed olefin metathesis, *J. Am. Chem. Soc*. 2015, **137**, 2476–2479; (l) W. Pickhardt, S. Gratz and L. Borchardt, Direct mechanocatalysis: using milling balls as catalysts, *Chem. Eur. J.* 2020, **26**, 12903–12911; (m) L. Chen, M. Regan and J. Mack, The Choice is yours:

using liquid-assisted grinding to choose between products in the palladium-catalyzed dimerization of terminal alkynes, *ACS Catal*. 2016, **6**, 868–872. (n) G. Dayaker, D. Tan, N. Biggins, A. Shelam, J.-L. Do, A. D. Katsenis and T. Friščić, Catalytic room-temperature C–N coupling of amides and isocyanates by using mechanochemistry, *ChemSusChem*, 2020, **13**, 2966–2972.

12. (a) D. V. Aleksanyan, S. G. Churusova, R. R. Aysin, Z. S. Klemenkova, Y. V. Nelyubina and V. A. Kozlov, The first example of mechanochemical synthesis of organometallic pincer complexes, *Inorg. Chem. Commun.* 2017, **76**, 33–35; (b) J. G. Hernandez and C. Bolm, Mechanosynthesis and applications in C–H bond functionalisations under ball-milling conditions, *Chem. Commun*. 2015, **51**, 12582–12584; (c) M. Juribašić Kulcsár, I. Halasz, D. Babić, D. Cinčić, J. Plavec and M. Ćurić, Aging and ball-milling as low-energy and environmentally friendly methods for the synthesis of Pd(II) photosensitizers, *Organometallics* 2014, **33**, 1227–1234; (d) A. Bjelopetrović, S. Lukin, I. Halasz, K. Užarević, I. Đilović, D. Barišić, A. Budimir, M. Juribašić Kulcsár and M. Ćurić, Mechanism of mechanochemical C–H bond activation in an azobenzene substrate by Pd(II) catalysts, *Chem. Eur. J*. 2018, **24**, 10672–10682; (e) A. Bjelopetrović, M. Robić, D. Babić, M. Juribašić Kulcsár and M. Ćurić, Facile mechanochemical anion substitution in cyclopalladated azo-benzenes, *Organometallics* 2019, **38**, 4479–4484; (f) F. J. L. Inger, Z. X. Giustra, S. Novosedlik, A. Orthaber, P. J. Gates, P. Dyrager and L. T. Pylarski, Mechanochemical synthesis of (hetero)aryl Au(I) complexes, *Green Chem*. 2020, 22, 5648–5655.
13. (a) G. N. Hermann, M. T. Unruh, S. H. Jung, M. Krings and C. Bolm, Mechanochemical rhodium(III)- and gold(I)-catalyzed C–H bond alkynylations of indoles under solventless conditions in mixer mills, *Angew. Chem., Int. Ed*. 2018, **57**, 10723−10727; (b) H. Cheng, J. G. Hernández and C. Bolm, Mechanochemical ruthenium-catalyzed hydroarylations of alkynes under ball-milling conditions, *Org. Lett*. 2017, **19**, 6284−6287; (c) H. Cheng, J. G. Hernández and C. Bolm, Mechanochemical cobalt-catalyzed C−H bond functionalizations by ball milling, *Adv. Synth. Catal*. 2018, **360**, 1800−1804; (d) G. N. Hermann and C. Bolm, Mechanochemical rhodium(III)-catalyzed C–H bond amidation of arenes with dioxazolones under solventless conditions in a ball mill, *ACS Catal.* 2017, **7**, 4592–4596; (e) G. N. Hermann, C. L. Jung and C. Bolm, Mechanochemical indole synthesis by rhodium-catalysed oxidative coupling of acetanilides and alkynes under solventless conditions in a ball mill, *Green Chem.* 2017, **19**, 2520–2523; (f) G. N. Hermann, P. B. Becker and C. Bolm, Mechanochemical iridium(III)-catalyzed C−H bond amidation of benzamides with sulfonyl azides under solvent-free conditions in a ball mill, *Angew*. *Chem. Int. Ed*. 2016, **55**, 3781–3784; (g) G. N. Hermann, P. B. Becker and C. Bolm, Mechanochemical rhodium(III)-catalyzed C–H bond functionalization of acetanilides under solventless conditions in a ball mill, *Angew*. *Chem. Int. Ed*. 2015, **54**, 7414–7417; (h) K.-Y. Jia, J.-B. Yu, Z.-J. Jiang and W.-K. Su, *J.* Mechanochemically activated oxidative coupling of indoles with acrylates through C–H activation: synthesis of 3-vinylindoles and β,β-diindolyl propionates and study of the mechanism, *J. Org. Chem*. 2016, **81**, 6049–6055; (i) S.-J. Lou, Y.-J. Mao, D.-Q. Xu, J.-Q. He, Q. Chen and Z.-Y. Xu, Fast and selective dehydrogenative C–H/C–H arylation using mechanochemistry, *ACS Catal*. 2016, **6**, 3890–3894; (j) Z. Liu, H. Xu

and Z.-Y. Wang, Palladium-catalyzed *ortho*-halogenations of acetanilides with *N*-halosuccinimides via direct sp^2 C–H bond activation in ball mills, *Beilstein J. Org. Chem*. 2018**, 14**, 430–435; (k) J. Yu, X. Yang, C. Wu and W. Su, Palladium-catalyzed C–H/C–H cross-coupling by mechanochemistry: direct alkenylation and heteroarylation of N1-protected 1*H*-indazoles, *J. Org. Chem*. 2020, **85**, 1009−1021.

14. M. Juribašić, K. Užarević, D. Gracin and M. Ćurić, Mechanochemical C–H bond activation: rapid and regioselective double cyclopalladation monitored by *in situ* Raman spectroscopy, *Chem. Commun.* 2014, **50**, 10287−10290.
15. (a) D. Gracin, V. Štrukil, I. Halasz and K. Užarević, Laboratory real-time and *in situ* monitoring of mechanochemical milling reactions by Raman spectroscopy, *Angew. Chem. Int. Ed.* 2014, **53**, 6193–6197; (b) L. Batzdorf, F. Fischer, M. Wilke, K.-J. Wenzel and F. Emmerling, Direct *in situ* investigation of milling reactions using combined X-ray diffraction and Raman spectroscopy, *Angew. Chem. Int. Ed.* 2015, ***54***, 1799–1802; (c) S. Lukin, T. Stolar, M. Tireli, M. V. Blanco, D. Babić, T. Friščić, K. Užarević and I. Halasz, Tandem *in situ* monitoring for quantitative assessment of mechanochemical reactions involving structurally unknown phases, *Chem. Eur. J.* 2017, **23**, 13941–13949.
16. X.-T. Ma and S.-K. Tian, Palladium-catalyzed regioselective halogenation of aromatic azo compounds, *Adv. Synth. Catal*. 2013, **355**, 337–340.
17. (a) M. D. K. Boele, G. P. F. van Strijdonck, A. H. M. de Vries, P. C. J. Kamer, J. G. de Vries and P. W. N. M. van Leeuwen, Selective Pd-catalyzed oxidative coupling of anilides with olefins through C–H bond activation at room temperature, *J. Am. Chem. Soc*. 2002, **124**, 1586–1587; (b) C. E. Houlden, C. D. Bailey, J. G. Ford, M. R. Gagne and G. C. Loyd-Jones, Distinct Reactivity of $Pd(OTs)_2$: the intermolecular Pd(II)-catalyzed 1,2-carboamination of dienes, *J. Am. Chem. Soc*. 2008, **130**, 10066–10067; (c) C. J. Mulligan, J. S. Parker and K. K. Hii, Revisiting the mechanism of the Fujiwara–Moritani reaction, *React. Chem. Eng*. 2020, **5**, 1104–1111.
18. E. Drent, J. A. M. van Broekhoven and M. J. Doyle, Efficient palladium catalysts for the copolymerization of carbon monoxide with olefins to produce perfectly alternating Polyketones, *J. Organomet. Chem*. 1991, **417**, 235–251.
19. V. Smrečki, G. Baranović, G. Keresztury and Z. Meić, Near-infrared Fourier transform Raman spectra of protonated and deuterated trans-azobenzene isotopomers, *J. Mol. Struct*. 1997, **408/409**, 405–408.
20. P. R. Patel, S. H. Henderson, M. S. Roe and M. A. Honey, Decarboxylative bromination of heteroarenes: initial mechanistic insights, *Synlett*, 2021, **31**, 1603–1607.
21. A. Bjelopetrović, D. Barišić, Z. Duvnjak, I. Džajić, M. Juribašić Kulcsár, I. Halasz, M. Martinez, A. Budimir, D. Babić and M. Ćurić, A detailed kinetico-mechanistic investigation on the palladium C–H bond activation in azobenzenes and their monopalladated derivatives, *Inorg. Chem*. 2020, 59, 17123–17133.
22. J. Tomasi, B. Mennucci and R. Cammi, Quantum mechanical continuum solvation models, *Chem. Rev.* 2005, **105**, 2999–3093.
23. B. S. Pladevall, A. de Aguirre and F. Maseras, Understanding ball milling mechanochemical processes with DFT calculations and microkinetic modeling, *ChemSusChem*, 2021, **14**, 2763–2768.

24. (a) D. C. Powers, D. Benitez, E. Tkatchouk, W. A. Goddard III and T. Ritter, Bimetallic reductive elimination from dinuclear Pd(III) complexes, *J. Am. Chem. Soc.* 2010, **132**, 14092–14103; (b) D. C. Powers, D. Y. Xiao, M. A. Geibel and T. Ritter, On the mechanism of palladium-catalyzed aromatic C–H oxidation, *J. Am. Chem. Soc.* 2010, **132**, 1453–1460.
25. (a) J. Duan, L. H. Zhang, W. R. Dolbier Jr., A convenient new method for the bromination of deactivated aromatic compounds, *Synlett*, 1999, 1245–1246; (b) K. Rajesh, M. Somasundaram, R. Saiganesh, K. K. Balasubramanian, Bromination of deactivated aromatics: a simple and efficient method, *J. Org. Chem.* 2007, **72**, 5867–5869;(c) H. Xue, H. Tan, D. Wei, Y. Wei, S. Lin, F. Liang, B. Zhao, *N*-Bromosuccinimide–carboxylic acid combination: mild and efficient access to dibromination of unsaturated carbonyl compounds, *RSC Advances*, 2013, **3**, 5382–5385; (d) B. Du, X. Jiang, P. Sun, Palladium-catalyzed highly selective ortho-halogenation (I, Br, Cl) of arylnitriles via sp^2 C–H bond activation using cyano as directing group, *J. Org. Chem.* 2013, **78**, 2786–2791.
26. B. E. Haines, H. Xu, P. Verma, P.; X.-C. Wang, J.-Q. Yu and D. G. Musaev, Mechanistic details of Pd(II)-catalyzed C–H iodination with molecular I_2: oxidative addition vs electrophilic cleavage, *J. Am. Chem. Soc.* 2015, **137**, 9022–9031.
27. S. F. Boys, Construction of some molecular orbitals to be approximately invariant for changes from one molecule to another, *Rev. Mod. Phys.* 1960, **32**, 296–299; (b) J. M Foster and S. F. Boys, Canonical configuration interaction procedure, *Rev. Mod. Phys.* 1960, **32**, 300–302.
28. A. V. Marenich, C. J. Cramer, D. G. Truhlar, Universal solvation model based on solute electron density and on a continuum model of the solvent defined by the bulk dielectric constant and atomic surface tensions, *J. Chem. Phys. B* 2009, **113**, 6378–6396.
29. (a) D. Babić, M. Ćurić and D. M. Smith, Computational study of the cyclopalladation mechanism of azobenzene with $PdCl_2$ in *N*,*N*-dimethylformamide, *J. Organomet. Chem.* 2011, **696**, 661–669; (b) M. Juribašić, A. Budimir, S. Kazazić and M. Ćurić, Dicyclopalladated complexes of asymmetrically substituted azobenzenes: synthesis, kinetics and mechanisms, *Inorg. Chem.* **2013**, *52*, 12749–12757.